ACADEMIC PRESS

Available online at www.sciencedirect.com

SCIENCE DIRECT®

Journal of Sound and Vibration 262 (2003) 633–649

JOURNAL OF SOUND AND VIBRATION

www.elsevier.com/locate/jsvi

Model reduction for parametric instability analysis in shells conveying fluid

Jayaraj Kochupillai, N. Ganesan, Chandramouli Padmanabhan*

Department of Applied Mechanics, Machine Dynamics Laboratory, Indian Institute of Technology Madras, Chennai 600 036, India

Received 19 November 2001; accepted 20 October 2002

Abstract

Flexible pipes conveying fluid are often subjected to parametric excitation due to time-periodic flow fluctuations. Such systems are known to exhibit complex instability phenomena such as divergence and coupled-mode flutter. Investigators have typically used weighted residual techniques, to reduce the continuous system model into a discrete model, based on approximation functions with global support, for carrying out stability analysis. While this approach is useful for straight pipes, modelling based on FEM is needed for the study of complicated piping systems, where the approximation functions used are local in support. However, the size of the problem is now significantly larger and for computationally efficient stability analysis, model reduction is necessary. In this paper, model reduction techniques are developed for the analysis of parametric instability in flexible pipes conveying fluids under a mean pressure. It is shown that only those linear transformations which leave the original eigenvalues of the linear time invariant system unchanged are admissible. The numerical technique developed by Friedmann and Hammond (Int. J. Numer. Methods Eng. Efficient 11 (1997) 1117) is used for the stability analysis. One of the key research issues is to establish criteria for deciding the basis vectors essential for an accurate stability analysis. This paper examines this issue in detail and proposes new guidelines for their selection.

1. Introduction

It is well established that under steady flow condition, pipes conveying fluids can undergo divergence and flutter type of instabilities. This usually happens at high flow velocities and is a function of the support conditions. In the case of pulsating fluids, parametric instability can occur at lower flow velocities depending on the amplitude and frequency of the velocity fluctuation. In

*Corresponding author. Tel.: +91-44-2257-8192; fax: +91-44-2257-0509.
E-mail address: mouli@iitm.ac.in (C. Padmanabhan).

0022-460X/03/$ - see front matter
doi:10.1016/S0022-460X(03)00115-9

the present study, the pulsation of the fluid is assumed to be harmonic about a mean flow velocity. Detailed investigations have been conducted by Païdoussis and Issid [1], Ginsberg [2], Chen [3] and Païdoussis and Sundararajan [4]. They have studied parametric instability of simple pipe structures using global approximations in a weighted residual procedure. In the review paper by Païdoussis and Li [5] a detailed description of almost all types of problems related to pipes conveying fluid is discussed. In the recent book by Païdoussis [6], greater insight into the physics of the problem is provided.

Most of the theoretical work on the dynamic stability of pipes has been concerned with linearized analytical models. Zhang et al. [7] presented a finite element model, based on Sanders' non-linear theory of thin shells and the classical potential theory for vibration of initially tensioned thin-walled orthotropic cylindrical tubes conveying fluid. They used a hydrodynamic pressure formulation derived from the velocity potential, a dynamic coupling condition at the fluid–structure interface, a non-linear strain–displacement relationship for the geometric stiffness matrix due to initial stresses and hydrostatic pressures, and two-noded frustrum elements to model the system. Hansson and Sandberg [8] developed a finite element model by combining an axi-symmetric shell element and a one-dimensional fluid element taking into consideration the interaction between the shell and the fluid. Weaver and Unny [9] used the Flügge–Kempner equation in conjunction with classical potential theory to model shells conveying fluids. Païdoussis et al. [10] presented an analytical model for the dynamics and stability of coaxial cylindrical shells conveying incompressible or compressible fluid in the inner shell and the annulus between the two shells. They used Flügge's thin-shell theory to model the shell and linearized potential flow theory for the fluid. Chang and Chiou [11] derived the equations of motion using Hamilton's principle and exploiting superposition, the natural frequencies corresponding to each flow velocity were found. Selman and Lakis [12] presented a theory for the determination of the effects of a flowing fluid on the vibration characteristics of an open, anisotropic cylindrical shell submerged and subjected simultaneously to an internal and external flow. Olson and Jamaison [13] compared the theoretical and finite element results for four test cases: a simplified cantilever pipe, a fixed–fixed pipe (clamped at both ends), a cantilever pipe and a spring supported cantilever pipe. Kock and Olson [14], Nitikitpaibon and Bathe [15] and Olson and Bathe [16] have developed finite element models to solve fluid–structure interaction problems. Jayaraman and Narayanan [17] investigated the chaotic motions of a simply supported non-linear pipe conveying fluid with harmonic velocity fluctuations. They observed both period doubling sequence and a sudden transition to chaos of an asymmetric period 2 motion near critical velocity for divergence. Païdoussis and Moon [18] have investigated theoretically and experimentally the chaotic behavior of a cantilevered pipe conveying fluid where the non-linearity is induced by motion limiting constraints.

Model reduction to analyze large systems has been reported by Bazoune et al. [19]. They overcame the problem of large dimensionality resulting from the finite element discretization by transforming from the space of nodal co-ordinates to the space of modal co-ordinates. This is used to find out the dynamic response of spinning tapered Timoshenko beams. Accuracy of the reduced model is demonstrated by comparing with the full model. Zhang et al. [20] developed a viscoelastic finite element model for the dynamic analysis of viscoelastic tubes conveying fluid, including the transverse shear and rotary inertia effects. For both viscoelastic and elastic models, they conducted modal and damping analysis for various initial axial tensions and fluid flow velocities. While these researchers have used the modal reduction technique for finding vibration

response, use of this technique to find the stability of large size problems is not found in the literature. Also Ritz and Lanczos vectors have been extensively used as a reduced basis for finding forced response of structures, but the suitability of these vectors for stability analysis has not been examined.

Most investigators have studied parametric instability of simple structures, using a one mode or two-mode global Galerkin approximation. In the present paper a coupled semi-analytical finite element formulation for the shell conveying fluid is presented. Thick shell theory is used to formulate the finite element equation of the structure while the fluid part is modelled by the Laplace equation. The fluid part is modelled using a velocity potential formulation and the dynamic pressure acting on the walls is derived from the Bernoulli's equation. Impermeability and dynamic condition are imposed on the fluid–structure interface. In the case of pulsating flow, some of the matrices become time dependent. To perform a stability analysis without numerical difficulties, modal reduction is carried out using the time invariant matrices of the time varying system. The coupled fluid–structure mode shapes are used for this purpose, which preserves the stability information. It is shown that only those linear transformations which preserve the eigenvalues are allowed for stability analysis. The reduced system stability analysis is carried out using Floquet–Liapunov theory and is shown to be computationally efficient.

2. Finite element formulation

2.1. Structure

A coupled semi-analytical finite element formulation for fluid–structure interaction is developed in this section. The general shell finite element formulation developed by Ramasamy and Ganesan [21] for viscoelastic shells, based on the displacement field proposed by Wilkins et al. [22], is used. Fig. 1 shows the schematic of the viscoelastic shell structure, consisting of a core viscoelastic layer sandwiched between two facing layers. For the core layer the displacement relations are assumed to be

$$u^c = u_0 + z\psi_s, \quad v^c = v_0 + z\psi_\theta, \quad w^c = w_0, \tag{1}$$

where u^c, v^c and w^c are the total displacements in the s, θ, and z directions and are defined in terms of the middle surface displacements u_0, v_0 and w_0 and the angles of rotations normal to the

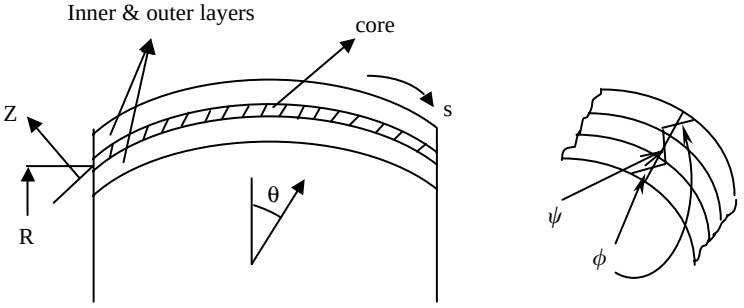

Fig. 1. Viscoelastic structure schematic.

middle surface in the meridional and circumferential directions. For the core these angles are denoted by ψ_s, ψ_θ while for the facings the angles are denoted by ϕ_s, ϕ_θ. For outer and inner facing, respectively, the displacements are related to the angles as

$$u^{fo}, u^{fi} = u_0 \pm h\psi_s + (z \pm h)\phi_s, \quad v^{fo}, v^{fi} = v_0 \pm h\psi_\theta + (z \pm h)\phi_\theta, \quad w^{fo}, w^{fi} = w_0. \tag{2}$$

Here 'z' denotes the distance from the middle surface of the shell, 'h' is half the core thickness. The strain displacement relations for the core becomes with $k_1 = 1/(1 + z/R_\phi)$ and R_ϕ being the radius of curvature:

$$\varepsilon^c_{ss} = k_1\left(\frac{\partial u_0}{\partial s} + \frac{w_0}{R_\phi} + z\frac{\partial \psi_s}{\partial s}\right),$$

$$\varepsilon^c_{\theta\theta} = k_2\left[\frac{1}{r}\frac{\partial v_0}{\partial \theta} + \frac{u_0}{r}\cos\phi + \frac{w_0}{r}\sin\phi + z\left(\frac{1}{r}\frac{\partial \psi_\theta}{\partial \theta} + \frac{\psi_s}{r}\cos\phi\right)\right], \tag{3}$$

$$\gamma^c_{s\theta} = k_1k_2\left[\frac{1}{r}\frac{\partial u_0}{\partial \theta} + \frac{\partial v_0}{\partial s} - \frac{v_0}{r}\cos\phi + z\left(\frac{1}{r}\frac{\partial \psi_s}{\partial \theta} + \frac{\partial \psi_\theta}{\partial s} - \frac{\psi_\theta}{r}\cos\phi\right)\right], \tag{4}$$

$$\gamma^c_{sz} = k_1\left[\psi_s - \frac{u_0}{R_\phi} + \frac{\partial w_0}{\partial s} + z\left(-\frac{\psi_s}{R_\phi}\right)\right],$$

$$\gamma^c_{\theta z} = k_2\left[\psi_\theta - \frac{v_0}{r}\sin\phi + \frac{1}{r}\frac{\partial w_0}{\partial \theta} + z\left(-\frac{\psi_\theta}{r}\sin\phi\right)\right]. \tag{5}$$

For the inner and outer facings, strain displacement relations are used as given in Ref. [21]. It is clear from the above relations that the degrees of freedom (d.o.f.) are $u_0, v_0, w_0, \psi_s, \psi_\theta, \phi_s$ and ϕ_θ. In the semi-analytical formulation, the circumferential variation of the seven variables (along θ) is expressed as a Fourier series,

$$\begin{Bmatrix} u_0 \\ v_0 \\ w_0 \\ \psi_s \\ \psi_\theta \\ \phi_s \\ \phi_\theta \end{Bmatrix} = \sum_{i=1}^{3}\sum_{n=0}^{\infty}[\bar{\theta}]\begin{Bmatrix} N_i\ u_{0n,i} \\ N_i\ v_{0n,i} \\ N_i\ w_{0n,i} \\ N_i\ \psi_{sn,i} \\ N_i\ \psi_{\theta n,i} \\ N_i\ \phi_{sn,i} \\ N_i\ \phi_{\theta n,i} \end{Bmatrix}, \tag{6}$$

where $[\bar{\theta}]$ is defined as

$$[\bar{\theta}] = \begin{bmatrix} c & & & & & & \\ & s & & & & & \\ & & c & & & & \\ & & & c & & & \\ & & & & s & & \\ & & & & & s & \\ & & & & & & c \end{bmatrix}, \tag{7}$$

where $c = \cos n\theta$, $s = \sin n\theta$, and where 'n' is the circumferential mode number, N_i are the shape functions used in finite element formulation given by $N_1 = (\xi^2 - \xi)/2$, $N_2 = 1 - \xi^2$, $N_3 = (\xi^2 + \xi)/2$, where $\xi = s/l$ is the iso-parametric axial co-ordinate and l is the length of the element. Now one can write the displacement vector as $\{\mathbf{u}\} = [\mathbf{N}]\{\mathbf{u}_e\}$, where $\{\mathbf{u}\}^{\mathrm{T}} = \{u^c\ v^c\ w^c\}$ for the core and $\{\mathbf{u}\}^{\mathrm{T}} = \{u^{fo/fi}\ v^{fo/fi}\ w^{fo/fi}\}$ for the facings. The strain vectors can be represented as $\{\varepsilon\} = \{\varepsilon_{ss}\ \varepsilon_{\theta\theta}\ \gamma_{s\theta}\ \gamma_{\theta z}\ \gamma_{sz}\} = [\mathbf{B}]\{\mathbf{u}_e\}$, where $[\mathbf{B}]$ is the strain displacement matrix. The elemental stiffness $[\mathbf{K}_e]$ and mass $[\mathbf{m}_e]$ matrices are then obtained from the following:

$$[\mathbf{K}_e] = \int_v [\mathbf{B}]^{\mathrm{T}}[\mathbf{D}][\mathbf{B}]\,\mathrm{d}v, \quad [\mathbf{m}_e] = \rho \int_v [\mathbf{N}]^{\mathrm{T}}[\mathbf{N}]\,\mathrm{d}v, \tag{8}$$

$$[\mathbf{D}] = \begin{bmatrix} \bar{\mathbf{Q}}_{11} & \bar{\mathbf{Q}}_{12} & \bar{\mathbf{Q}}_{16} & 0 & 0 \\ & \bar{\mathbf{Q}}_{22} & \bar{\mathbf{Q}}_{26} & 0 & 0 \\ & & \bar{\mathbf{Q}}_{66} & 0 & 0 \\ & \textit{Sym.} & & \bar{\mathbf{Q}}_{44} & \\ & & & & \bar{\mathbf{Q}}_{55} \end{bmatrix}, \quad \bar{\mathbf{Q}} = [\mathbf{T}]^{\mathrm{T}}[\mathbf{Q}][\mathbf{T}], \tag{9}$$

where $[\mathbf{Q}]$ is the elasticity matrix in the material co-ordinates, $[\bar{\mathbf{Q}}]$ is the transformed elasticity matrix in global co-ordinates and $[\mathbf{T}]$ is the standard transformation matrix. The elements of $[\mathbf{Q}]$ are given by $Q_{11} = E_L/(1 - \gamma_{LT}\gamma_{TL})$, $Q_{12} = \gamma_{TL}Q_{11}$, $Q_{22} = E_T/(1 - \gamma_{LT}\gamma_{TL})$, $Q_{66} = G_{LT}$, $Q_{44} = G_{TZ}$, and $Q_{55} = G_{LZ}$. Numerical integration using Gauss quadrature scheme is carried out for Eq. (8). If the same material is used for all the three layers, the above formulation will reduce to first order shear deformation theory and if curvature is only in one direction, the shell becomes a cylinder.

2.2. Fluid domain

A semi-analytical, eight noded, annular, isoparametric element is used for modelling the fluid domain. The governing differential equation for the fluid region is the Laplace equation. Its finite element form has velocity potential as the nodal d.o.f. The pressure in excess of hydrostatic pressure, p, is associated with the motion of the fluid. This pressure is given by the Bernoulli's equation. Fig. 2 shows a typical discretization of the structure and fluid. The following assumptions were made in deriving the equations: (1) the fluid flow is potential, (2) small deformations for the structure, (3) flow is inviscid, irrotational and isentropic and fluid pressure is

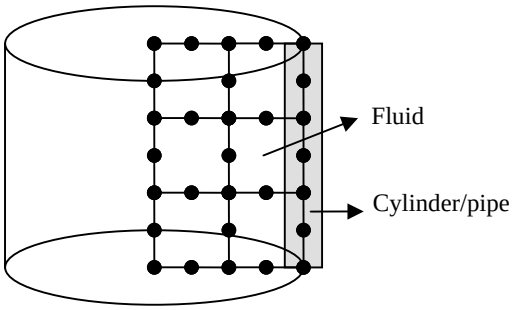

Fig. 2. Typical discretization of structure (3 nodes) and fluid (8 nodes).

normal to the shell wall, (4) fluid is incompressible and (5) no flow separation or cavitation. The mean pressure $\bar{p}$ will be taken as a load acting normal to the inside shell surface. Further, the velocity potential should satisfy the Laplace equation (in cylindrical co-ordinates):

$$\frac{1}{r}\frac{\partial}{\partial r}\left(r\frac{\partial\phi}{\partial r}\right)+\frac{1}{r^2}\frac{\partial^2\phi}{\partial\theta^2}+\frac{\partial^2\phi}{\partial x^2}=0, \tag{10}$$

where ϕ is the velocity potential and the boundary conditions. The weak form of Eq. (10) is used to formulate the finite element matrices.

2.3. Coupled fluid–structure system

The radial velocity of the fluid must be equal to the instantaneous velocity of the shell. This will satisfy the impermeability or dynamic boundary conditions, which ensures contact between the shell and the fluid. This implies that the radial velocity of the fluid and structure are the same at the interface:

$$V_r=\left.\frac{\partial\phi}{\partial r}\right|_{r=R}=\frac{\partial w}{\partial t}+U_x\frac{\partial w}{\partial x}. \tag{11}$$

The dynamic pressure acting on the shell surface is given by Bernoulli's equation for unsteady flow,

$$p=-\rho\left(\frac{\partial\phi}{\partial t}+U_x\frac{\partial\phi}{\partial x}\right). \tag{12}$$

The weak form of the Laplace equation is used to formulate the finite element matrices. Making use of Eq. (11) at the fluid–structure interface one obtains

$$\int_S N_f^{\mathrm{T}}\nabla\phi.\hat{n}\,\mathrm{d}S=\int N_f^{\mathrm{T}}\bar{N}\,\mathrm{d}s\{\dot{u}_e\}+U_x\int N_f^{\mathrm{T}}\frac{\partial\bar{N}}{\partial x}\,\mathrm{d}S\{u_e\}, \tag{13}$$

where $\bar{N}$ is the w component of the shell shape function and $\hat{n}$ is the unit normal component of the velocity potential to the structure. Similarly from Eq. (9), the pressure acting on the fluid–structure interface can be converted to the finite element equations

$$\int_S \bar{N}^{\mathrm{T}}\rho_f\left(\frac{\partial\phi}{\partial t}+U_x\frac{\partial\phi}{\partial x}\right)\mathrm{d}S=\rho_f\int_S\bar{N}^{\mathrm{T}}N_f\,\mathrm{d}S\{\dot{\phi}_e\}+\rho_f U_x\int_S\bar{N}^{\mathrm{T}}\frac{\partial N_f}{\partial x}\,\mathrm{d}S\{\phi_e\}. \tag{14}$$

Now the complete fluid–structure finite element equation is

$$\begin{bmatrix} \mathbf{M}^{uu} & \mathbf{0} \\ \mathbf{0} & \mathbf{0} \end{bmatrix} \begin{Bmatrix} \ddot{u} \\ \ddot{\phi} \end{Bmatrix} + \begin{bmatrix} \mathbf{0} & \mathbf{C}^{u\phi} \\ -\mathbf{C}^{\phi u} & \mathbf{0} \end{bmatrix} \begin{Bmatrix} \dot{u} \\ \dot{\phi} \end{Bmatrix} + \begin{bmatrix} \mathbf{K}^{uu} & U_x\mathbf{K}^{u\phi} \\ -U_x\mathbf{K}^{\phi u} & \mathbf{H}^{\phi\phi} \end{bmatrix} \begin{Bmatrix} u \\ \phi \end{Bmatrix} = \begin{Bmatrix} 0 \\ 0 \end{Bmatrix}. \tag{15}$$

The second row of Eq. (15) yields the relation

$$\{\phi\} = [\mathbf{H}^{\phi\phi}]^{-1}[\mathbf{C}^{\phi u}]\{\dot{u}\} + U_x[\mathbf{H}^{\phi\phi}]^{-1}[\mathbf{K}^{\phi u}]\{u\}. \tag{16}$$

The time derivative of potential is given by

$$\{\dot{\phi}\} = [\mathbf{H}^{\phi\phi}]^{-1}[\mathbf{C}^{\phi u}]\{\ddot{u}\} + U_x[\mathbf{H}^{\phi\phi}]^{-1}[\mathbf{K}^{\phi u}]\{\dot{u}\} + \dot{U}_x[\mathbf{H}^{\phi\phi}]^{-1}[\mathbf{K}^{\phi u}]\{u\}. \tag{17}$$

Substituting ϕ and $\dot{\phi}$ in the structural equation, we get

$$\begin{aligned}[\mathbf{M}^{uu} + \mathbf{C}^{u\phi}\mathbf{H}^{\phi\phi^{-1}}\mathbf{C}^{\phi u}]\{\ddot{u}\} + U_x[\mathbf{C}^{u\phi}\mathbf{H}^{\phi\phi^{-1}}\mathbf{K}^{\phi u} + \mathbf{K}^{u\phi}\mathbf{H}^{\phi\phi^{-1}}\mathbf{C}^{\phi u}]\{\dot{u}\} \\ + [\mathbf{K}^{uu} + U_x^2\mathbf{K}^{u\phi}\mathbf{H}^{\phi\phi^{-1}}\mathbf{K}^{\phi u} + \dot{U}_x\mathbf{K}^{u\phi}\mathbf{H}^{\phi\phi^{-1}}\mathbf{K}^{\phi u}]\{u\} = 0.\end{aligned} \tag{18}$$

The above equation can be written compactly as

$$[\mathbf{M}^*]\{\ddot{u}\} + U_x[\mathbf{C}^*]\{\dot{u}\} + [[\mathbf{K}^*] + U_x^2[\tilde{\mathbf{K}}] + \dot{U}_x[\tilde{\mathbf{K}}]]\{u\} = 0, \tag{19}$$

where $[\tilde{\mathbf{K}}] = [\mathbf{K}^{u\phi}\mathbf{H}^{\phi\phi-1}\mathbf{K}^{\phi u}]$. The elemental structural mass matrix is $\mathbf{m}_e = \rho\int_V \mathbf{N}^{\mathrm{T}}\mathbf{N}\,\mathrm{d}V$, with the global matrix on assembly being $\mathbf{M}^{uu}$ elemental fluid–structure coupling matrices are $\mathbf{C}_e^{u\phi} = \rho_f\int_S \bar{\mathbf{N}}^{\mathrm{T}}\mathbf{N}_f\,\mathrm{d}S$ and $\mathbf{C}_e^{\phi u} = \int_S \mathbf{N}_f^{\mathrm{T}}\bar{\mathbf{N}}\,\mathrm{d}S$, the elemental Coriolis fluid energy matrix normalized with respect to mean flow velocity is $\mathbf{C}_e^{\phi\phi} = 2/c^2\int_V \mathbf{N}_f^{\mathrm{T}}(\partial\mathbf{N}_f/\partial x)\,\mathrm{d}V$, the structural stiffness matrix $\mathbf{K}_e^{uu} = \int_V \mathbf{B}^{\mathrm{T}}\mathbf{D}\mathbf{B}\,\mathrm{d}V$. The elemental stiffness coupling matrices due to flow are $\mathbf{K}_e^{u\phi} = \rho_f\int_S \bar{\mathbf{N}}^{\mathrm{T}}(\partial\mathbf{N}_f/\partial x)\,\mathrm{d}S$ and $\mathbf{K}_e^{\phi u} = \int_S \mathbf{N}_f^{\mathrm{T}}(\partial\bar{\mathbf{N}}/\partial x)\,\mathrm{d}S$ and the matrix representing the kinetic energy in a fluid element is $\mathbf{H}_e^{\phi\phi} = \int_V \nabla\mathbf{N}_f^{\mathrm{T}}\nabla\mathbf{N}_f\,\mathrm{d}V$. In this case, an added mass term, an added damping term due to potential formulation (Coriolis effect) and an added stiffness term due to stiffening by the pressure acting on the walls (centrifugal force) is present. In the case of pulsating flow, the velocity of flow is given as $U_x = U_0(1 + \mu\cos\Omega t)$. Substituting this into Eq. (19), one gets

$$\begin{aligned}[\mathbf{M}^*]\{\ddot{u}\} + U_0[\mathbf{C}^*]\{\dot{u}\} + \left[[\mathbf{K}^*] + U_0^2\left(1 + \frac{\mu^2}{2}\right)[\tilde{\mathbf{K}}]\right]\{u\} \\ + U_0\mu\cos\Omega t[\mathbf{C}^*]\{\dot{u}\} + U_0^2\mu\left(2\cos\Omega t + \frac{\mu}{2}\cos 2\Omega t - \frac{\Omega}{U_0}\sin\Omega t\right)[\tilde{\mathbf{K}}]\{u\} = 0.\end{aligned} \tag{20}$$

2.4. Stability analysis

Friedmann and Hammond [23], had proposed an improved numerical integration scheme for obtaining the transition matrix for large size problems. The transition or monodromy matrix is calculated using a fourth order Runge–Kutta scheme with Gill coefficients. Eq. (20) can be written as an equation of motion having time-dependent coefficients,

$$[\mathbf{M}]\{\ddot{x}\} + [\mathbf{C}(t)]\{\dot{x}\} + [\mathbf{K}(t)]\{x\} = 0. \tag{21}$$

The reduced equation is written in the state space form as

$$\{\dot{v}\} = [\mathbf{A}(t)]\{v\} = \{f(t, v)\}, \tag{22}$$

where

$$[\mathbf{A}(t)] = \begin{bmatrix} 0 & \mathbf{I} \\ -[\mathbf{M}]^{-1}[\mathbf{K}(t)] & -[\mathbf{M}]^{-1}[\mathbf{C}(t)] \end{bmatrix} \quad \text{and} \quad \{v\} = \begin{Bmatrix} x \\ \dot{x} \end{Bmatrix}.$$

The Floquet–Liapunov theory states that knowledge of the state transition matrix over one period is sufficient in order to determine the stability of a periodic system, Eq. (22), where $[\mathbf{A}(t)] = [\mathbf{A}(t+T)]$ is the periodic matrix. The Floquet–Liapunov theorem provides extremely valuable information about the form and properties of the solution, even though it does not yield a solution. The knowledge of the transition matrix over one period determines the solution to the homogeneous system. The stability criteria for the system is derived from the real parts of eigenvalues of the transition matrix. If the magnitude of the eigenvalues is less than 1 the system is stable, else the system is not stable.

The fourth order Runge–Kutta method with Gill coefficients has been used by Friedmann and Hammond [23] to generate the monodromy or transition matrix based on integration over one time period T:

$$[\varphi_A(T,0)] = \prod_{i=1}^{N} [B(T-ih)], \quad h = T/N, \tag{23}$$

$$[B(t_i)] = [I] + \frac{h}{6}\left([A(t_i)] + 2\left(1 - \frac{1}{\sqrt{2}}\right)[E(t_i)] + 2\left(1 + \frac{1}{\sqrt{2}}\right)[F(t_i)] + [G(t_i)]\right), \tag{24}$$

$$[E(t_i)] = \left[A\left(t_i + \frac{h}{2}\right)\right]\left([I] + \frac{1}{2}h[A(t_i)]\right), \tag{25}$$

$$[F(t_i)] = \left[A\left(t_i + \frac{h}{2}\right)\right]\left([I] + \left(-\frac{1}{2} + \frac{1}{\sqrt{2}}\right)h[A(t_i)] + \left(1 - \frac{1}{\sqrt{2}}\right)h[E(t_i)]\right), \tag{26}$$

$$[G(t_i)] = [A(t_i + h)]\left([I] - \frac{h}{\sqrt{2}}[E(t_i)] + \left(1 + \frac{1}{\sqrt{2}}\right)h[F(t_i)]\right). \tag{27}$$

3. Model reduction

The stability analysis of the shell conveying pulsating fluid could not be carried out on the full model, irrespective of the mesh size and time step used because of the numerical overflow problem. The method suggested by Friedmann and Hammond [23] for stability analysis involves a large number of multiplications and therefore numerical problems such as overflow errors occur. This problem could not be overcome even with lesser number of elements and larger number of time steps. However, to ensure a reasonable accuracy of results for complex structures, coarse discretization may not be sufficient. It is clear that in order to study the stability of a pipe conveying pulsating fluid discretized using the finite element method, a full model cannot be used. Therefore, there exists a need to reduce the size of the problem. To achieve this goal a co-ordinate

transformation to the modal domain is made using the first few eigenvectors of the time invariant system. This reduces the number of d.o.f. of the system, without losing the stability information. In the present case, the free vibration mode shape of the steady flow case (linear time invariant part of Eq. (20)) is chosen for transforming the system to the modal co-ordinates. The finite element equation of the steady flow pipe without considering damping is

$$[\mathbf{M}^*]\{\ddot{u}\} + \left[\mathbf{K}^* + U_0^2\left(1 + \frac{\mu^2}{2}\right)\tilde{\mathbf{K}}\right]\{u\} = \{0\}. \tag{28}$$

Using the LAPACK [24] routine DSYGV, the eigenvectors $[\psi]$ of Eq. (28) are found. These eigenvectors are orthogonal with respect to $[\mathbf{M}^*]$ and $[\mathbf{K}^* + U_0^2(1 + \mu^2/2)\mathbf{F}]$. Using the transformation $u = [\psi]\{x\}$ in the full Eq. (20) and pre-multiplying by $[\psi^{\mathrm{T}}]$ the resulting matrix can be written as

$$[\mathbf{M}^r]\{\ddot{x}\} + [\mathbf{C}^r(t)]\{\dot{x}\} + [\mathbf{K}^r(t)]\{x\} = \{0\}, \tag{29}$$

where

$$[\mathbf{M}^r] = [\psi]^{\mathrm{T}}[\mathbf{M}][\psi] = [\mathbf{I}], \quad [\mathbf{C}^r(t)] = U_0(1 + \mu\cos\Omega t)[\psi]^{\mathrm{T}}[\mathbf{C}^*][\psi],$$

$$[\mathbf{K}^r(t)] = [\psi]^{\mathrm{T}}\left[[\mathbf{K}^*] + U_0^2\left(1 + \frac{\mu^2}{2} + 2\mu\cos\Omega t + \frac{\mu^2}{2}\cos 2\Omega t - \frac{\mu}{U_0}\Omega\sin\Omega t\right)[\tilde{\mathbf{K}}]\right][\psi].$$

Here the matrix $[\mathbf{M}^r]$ is the identity matrix, but $[\mathbf{C}^r(t)]$ and $[\mathbf{K}^r(t)]$ are not diagonal matrices. However, the matrices are now considerably smaller when compared to the original problem. Due to these reasons the numerical computation should not pose any difficulties. Further during the normalization process, the stiffness coefficients become much smaller (from $O(10^9)$ to $O(10^3)$ and mass coefficients increase from $O(10^{-3})$ to $O(1)$.

4. Validation

Chen's [3] book on flow-induced vibration presented a detailed investigation of the flow-induced vibration of cylindrical structures, while Païdoussis [6] presented the static and dynamic instabilities of pipes conveying fluids. Both assume an incompressible, inviscid, isentropic plug flow. Their formulation for the structure is based on Euler beam theory. In the present shell formulation, the degrees of freedom in the radial and circumferential directions are decoupled by the use of the semi-analytical technique. Hence the results for the circumferential mode $n = 1$ which corresponds to the beam mode, is validated with those of Païdoussis [6] which is also referenced in Refs. [3,5,25]. These results are for two different values of non-dimensional parameter β with the clamped–clamped boundary condition. The parameter β represents the ratio of the fluid mass to the sum of structural and the fluid masses. Using the shell formulation, results are generated for the clamped–clamped boundary condition and for the same β values ($\beta = 0.1$ and $\beta = 0.8$). These are shown in Figs. 3 and 4. These figures show the dimensionless flow velocity u versus the dimensionless frequency ω/ω_0, where ω is the frequency of the structure in rad/s, ω_0 is $\sqrt{(EI/(m + m_f)L^4)}$ and u is $U_x/\sqrt{(EI/m_f L^2)}$ where U_x is the flow velocity in m/s, m is mass per unit length of pipe (kg/m), m_f is the mass per unit length of fluid (kg/m) and L is the length of pipe in meters. For $\beta = 0.1$, the divergence occurs first when the flow velocity reaches 6.28 and if

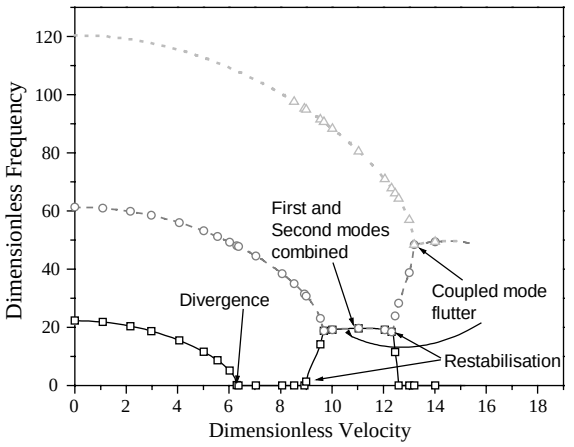

Fig. 3. Comparison of results of Païdoussis [6] and the present formulation for $\beta = 0.8$. Present: ——, $n = 1,\ m = 1$; - - - -, $n = 1,\ m = 2$; ....., $n = 1,\ m = 3$. Paidoussis [6]: □, $m = 1$; ○, $m = 2$; △, $m = 3$.

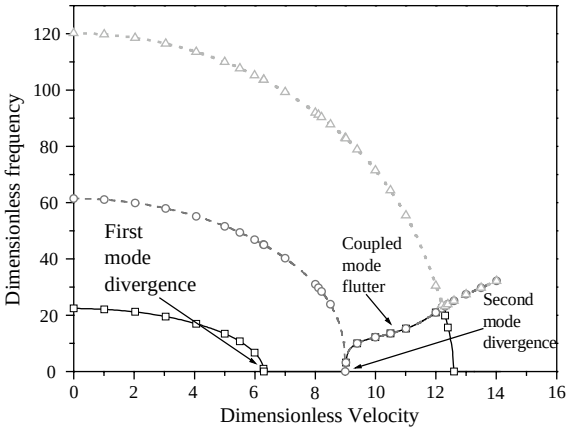

Fig. 4. Comparison of results of Païdoussis [6] and the present formulation for $\beta = 0.1$. Present: ——, $n = 1,\ m = 1$; - - - -, $n = 1,\ m = 2$; ....., $n = 1,\ m = 3$. Paidoussis [6]: □, $m = 1$; ○, $m = 2$; △, $m = 3$.

the flow velocity is increased further the second mode divergence occurs at flow velocity of 8.99. Upon further increasing the flow velocity the first and second mode frequencies increases together and joins with the third mode. Coupled mode flutter occurs here. The first mode then decreases to zero and the second and third move together to the fourth mode. In the case of $\beta = 0.8$, there is a stability region between $u = 8.99$ and 9.6. From both the figures, it is clear that the present formulation provides excellent agreement with the results of Païdoussis [6]. It must be pointed out that not only do the curves match well but the various physical phenomena that occur in these results have been correctly predicted by the current shell formulation. This then validates the use of the shell formulation.

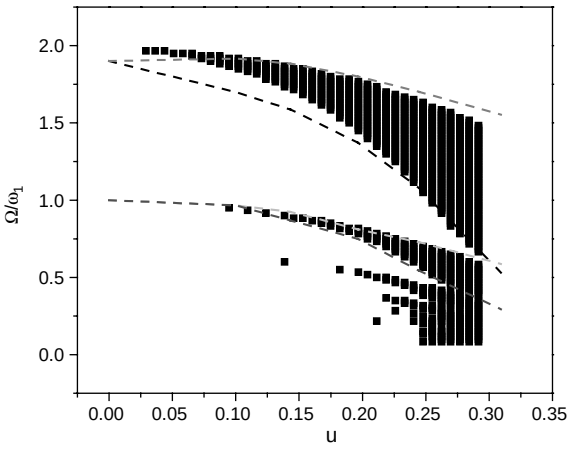

Fig. 5. Comparison of the results of Ginsberg with the present results for stability of the first mode: ■, present; - - -, Ginsberg [2].

Ginsberg [2] derived the differential equation for pipes conveying pulsating fluid. He used a two-mode Galerkin approximation considering the pipe as a beam. In the present study, the effects of the axial acceleration as discussed in Ref. [1] are not considered. The comparison of stability results with those of Ginsberg [2] is shown in Fig. 5. The scattered points which look like thick vertical lines corresponds to the present formulation while the dotted lines show Ginsberg's results. The present formulation predicts the almost the same instability regions as in Ref. [2]. Deviations in the results can be attributed to the fact that the mode shapes used to reduce the problem size in the present formulation includes the fluid–structure interaction effects, while Ginsberg's model is based only on the structural mode shape. One can state that the present result is more realistic.

5. Stability—eigenvector relationship

The influence of an eigenvector on the instability of the original system when it is reduced to a single-degree-of-freedom (s.d.o.f.) system based on that eigenvector is examined. The first five eigenvectors are selected for this and the results of these s.d.o.f. simulations are shown in Figs. 6–11, respectively. It is clear that the primary parametric instability is almost completely predicted by the first mode. The second and third modes show instability regions around $\Omega = 8$. Of course, this is very strong for mode 2. Mode 3 exhibits strong instability around $\Omega = 16$. Fig. 11 shows the instability of the system when these results are simply combined in one graph. Comparing Figs. 6–11 it is clear that they are almost the same. This implies that instability can be studied through several s.d.o.f. models for this system.

Figs. 12 and 13 show the instability region for the first mode for a value of $\mu = 0.8$. It is observed as expected that the instability region widens with a larger amplitude of fluctuation. One can use the finite element method to model the structure and the first few mode shapes (number depending on the excitation frequency) can be used for the co-ordinate transformation, which will

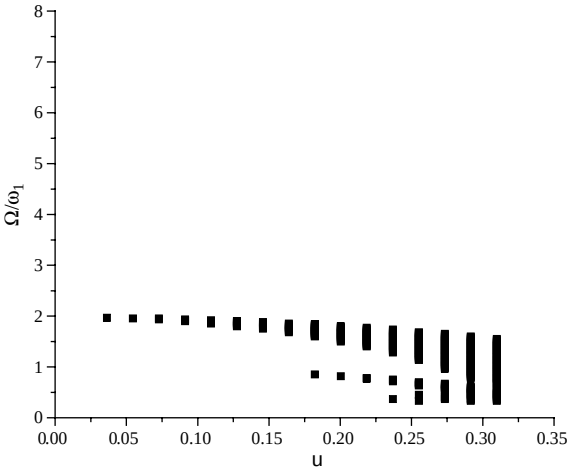

Fig. 6. Stability boundaries for the first mode approximation with $\mu = 0.4$.

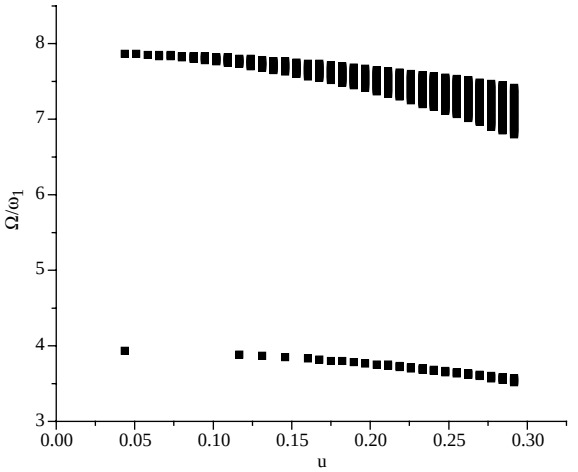

Fig. 7. Stability boundaries for the second mode approximation with $\mu = 0.4$.

make the problem size very small. In the modal domain also, the first degree of freedom corresponds to the first instability mode, the second degree of freedom for the second and so on. It is seen from Fig. 14 that the coupling effect is very weak in the case of $\mu = 0.8$ also.

6. Other transformations

Instead of eigenvectors, Ritz vectors and Lanczos vectors are used for the transformation to reduce the size of the matrix. These are carried out believing that the information of more than one mode will be present in the transformed matrix with lesser number of Ritz/Lanczos vectors.

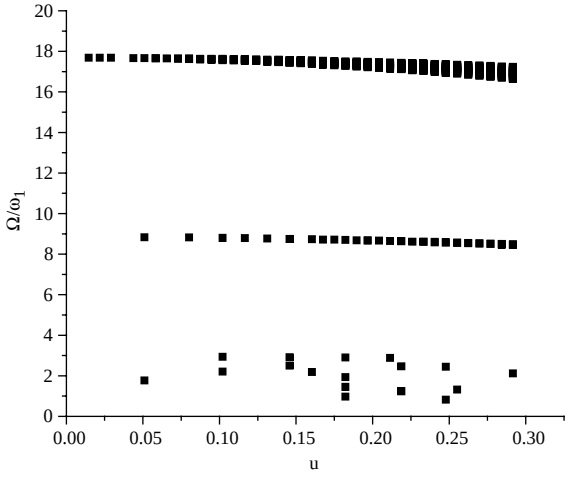

Fig. 8. Stability boundaries for the third mode approximation with $\mu = 0.4$.

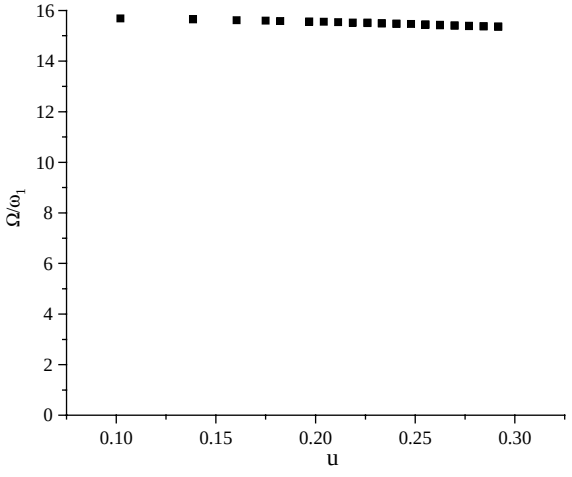

Fig. 9. Stability boundaries for the fourth mode approximation with $\mu = 0.4$.

However, the eigenvalues of the resulting matrix are not preserved with these types of transformations. Therefore, the instability boundaries, which depend on the eigenvalues also, are inaccurate. When the loading pattern for the Ritz vector corresponds to the first mode shape of the system, the subsequent Ritz vectors generated also correspond to the subsequent eigenvalues of the system. Hence the instability is predicted correctly. It is concluded from this study that only those transformations, which preserve the eigenvalues are useful for the stability analysis. In order to further verify this a linear combination of the eigenvectors is used for the transformation. The first two eigenvectors are combined as $0.5\psi_1 + 0.5\psi_2$ and used to transform the matrix, where ψ_1 and ψ_2 are the eigenvectors corresponding to the first two eigenvalues. In this case, the results

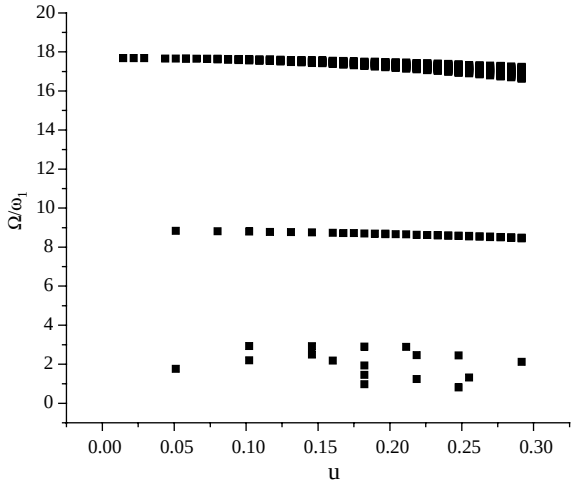

Fig. 10. Stability boundaries for the fifth mode approximation with $\mu = 0.4$.

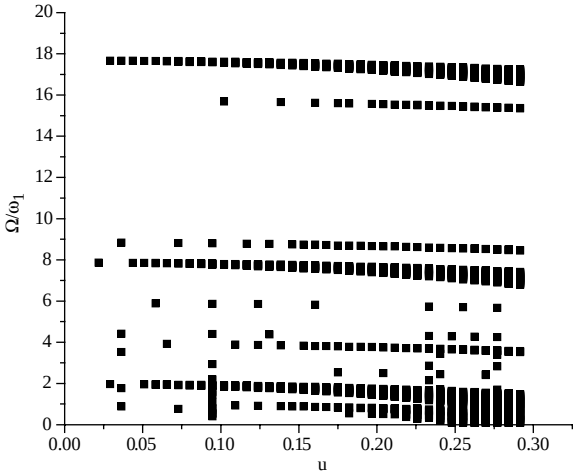

Fig. 11. Stability boundaries for the 5-d.o.f. reduced system with $\mu = 0.4$.

converge to fictitious eigenvalues, which do not represent the eigenvalues of the real system. Hence they cannot provide the correct instability boundaries.

7. Conclusions

A new efficient technique for the parametric instability analysis of complex shell structures conveying pulsating fluid is developed. The model is based on an elastic finite element formulation which has been validated with the published results. The reduced order model obtained using modal reduction has been successfully applied to the prediction of stability in a pipe conveying

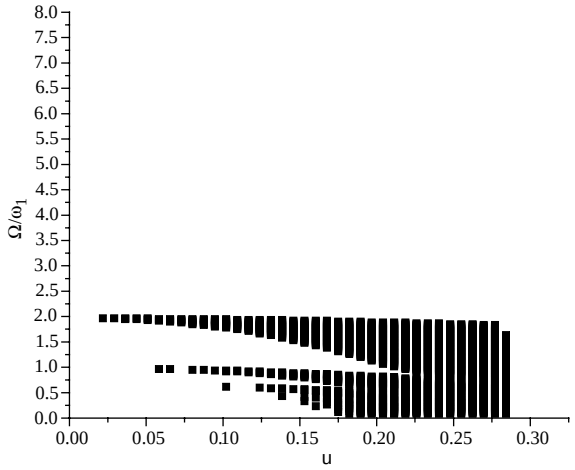

Fig. 12. Instability region for first mode with $\mu = 0.8$.

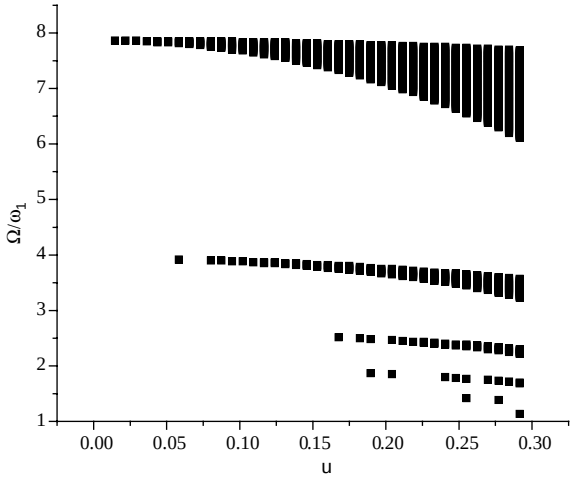

Fig. 13. Instability region for second mode with $\mu = 0.8$.

pulsating fluid. The few retained modes preserve the exact stability information of the pipe conveying pulsating fluid. Based on the results of simulation, it can be concluded that modal reduction can be used to alleviate the problem of large dimensionality resulting from the finite element discretization of complex structures. Other transformations for model reduction are looked into. It is understood that only the transformation, which preserves the eigenvalues, is useful for stability analysis. Another inference is that each of the decoupled s.d.o.f equations can be used for stability analysis corresponding to that particular eigenvalue. In the case of fluid–structure interaction problems, complex modal reduction would be expected to produce results that are more accurate and will be a useful extension to the present work. In complex modal reduction, the effect of the damping term, which represents the Coriolis effect of the fluid, is also

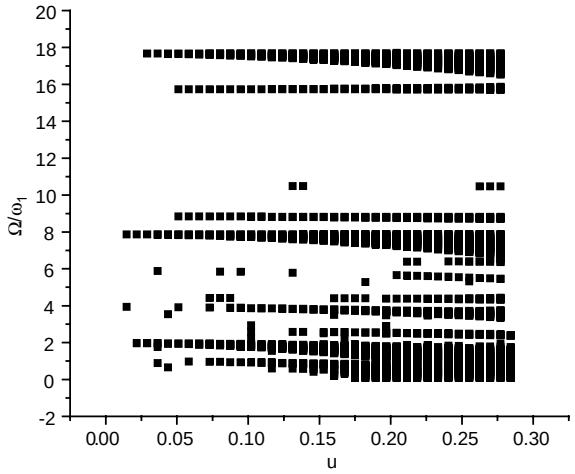

Fig. 14. Instability region for 4-d.o.f. reduced model with $\mu = 0.8$.

included in the eigenvalues problem. Therefore, it may be a more accurate representation of the real problem.

References

[1] M.P. Païdoussis, N.T. Issid, Dynamic stability of pipes conveying fluid, Journal of Sound and Vibration 33 (1974) 267–294.
[2] J.H. Ginsberg, The dynamic stability of a pipe conveying a pulsatile flow, International Journal of Engineering Science 11 (1973) 1013–1024.
[3] S.S. Chen, Flow Induced Vibration of Circular Cylindrical Structures, Hemisphere, New York, 1987.
[4] M.P. Païdoussis, Sundararajan, Parametric and combination resonance of a pipe conveying pulsating fluid, Journal of Applied Mechanics, American Society of Mechanical Engineers 42 (1975) 780–784.
[5] M.P. Païdoussis, G.X. Li, Pipes conveying fluid: a model dynamical problem, Journal of Fluids and Structures 7 (1993) 137–204.
[6] M.P. Païdoussis, Fluid–Structure Interactions: Slender Structures and Axial Flow, Vol. I, Academic Press, London, 1998.
[7] Y.L. Zhang, D.G. Gorman, J.M. Reese, A finite element method for modeling the vibration of initially tensioned thin-walled orthotropic cylindrical tubes conveying fluid, Journal of Sound and Vibration 245 (2001) 93–112.
[8] P.-A. Hansson, G. Sandberg, Dynamic finite element analysis of fluid-filled pipes, Computer Methods in Applied Mechanics and Engineering 190 (2001) 3111–3120.
[9] D.S. Weaver, T.E. Unny, On the dynamic stability of fluid-conveying pipes, Journal of Applied Mechanics, American Society of Mechanical Engineers 40 (1973) 48–52.
[10] M.P. Païdoussis, S.P. Chan, A.K. Misra, Dynamics and stability of coaxial cylindrical shells containing flowing fluid, Journal of Sound and Vibration 97 (1984) 201–235.
[11] J.-S. Chang, W.-J. Chiou, Natural frequencies and critical velocities of fixed–fixed laminated circular cylindrical shells conveying fluids, Computers and Structures 57 (1995) 929–939.
[12] A. Selman, A.A. Lakis, Vibration analysis of anisotropic open cylindrical shells subjected to flowing fluid, Journal of Fluids and Structures 11 (1997) 111–134.
[13] L.G. Olson, D. Jamison, Application of a general purpose finite element method to elastic pipes conveying fluid, Journal of Fluids and Structures 11 (1997) 207–222.

[14] E. Kock, L.G. Olson, Fluid structure interaction analysis by the finite element method. A variational approach, International Journal of Numerical Methods in Engineering 31 (1991) 463–491.
[15] C. Nitikitpaiboon, K.J. Bathe, An arbitrary Lagrangian–Eulerian velocity potential formulation for fluid structure interaction, Computers and Structures 47 (1993) 877–891.
[16] L.G. Olson, K.J. Bathe, Analysis of fluid–structure interaction. A direct symmetric coupled formulation based on the fluid velocity potential, Computers and Structures 21 (1985) 21–32.
[17] K. Jayaraman, S. Narayanan, Chaotic oscillations in pipes conveying pulsating fluid, Nonlinear Dynamics 10 (1996) 333–357.
[18] M.P. Païdoussis, F.C. Moon, Nonlinear and chaotic fluid elastic vibrations of a flexible pipe conveying fluid, Journal of Fluids and Structures 3 (1988) 567–591.
[19] A. Bazoune, Y.A. Khulief, N.G. Stephen, M.A. Mohiuddin, Dynamic response of spinning tapered Timoshenko beams using modal reduction, Finite Element Analysis in Design 37 (2001) 199–219.
[20] Y.L. Zhang, D.G. Gorman, J.M. Reese, A modal and damping analysis of viscoelastic Timoshenko tubes conveying fluid, International Journal of Numerical Methods in Engineering 50 (2001) 419–433.
[21] R. Ramasamy, N. Ganesan, Finite element analysis of fluid filled isotropic cylindrical shells with constrained viscoelastic damping, Computers and Structures 70 (1998) 363–376.
[22] D.J. Wilkins Jr., C.W. Bert, D.M. Egle, Free vibrations of orthotropic sandwich conical shells with various boundary conditions, Journal of Sound and Vibration 13 (1970) 211–228.
[23] P. Friedmann, C.E. Hammond, Numerical treatment of periodic systems with application to stability problems, International Journal of Numerical Methods in Engineering, Efficient 11 (1977) 1117–1136.
[24] E. Anderson, Z. Bai, C. Bischof, S. Blackford, J. Demmel, J. Dongarra, J. Du Croz, A. Greenbaum, S. Hammarling, A. Mckenney, D. Sorensen, LAPACK User's Guide, SIAM, Philadelphia, 1999.
[25] M.P. Païdoussis, Flow-induced instabilities of cylindrical structures, Applied Mechanics Reviews 40 (1987) 163–175.